Magnetic interaction in superparamagnetic Co-Pt nanoparticles synthesized in protein crystal

Kakeru Tagata[1], Daisuke Kanda[1], Naoto Kobayashi[1], Akifumi Higashiura[2], Satoshi Ichikawa[3], Noriaki Kishida[1], Ryoichi Nakatani[1,4,5], Atsushi Nakagawa[6], and Yu Shiratsuchi[1,4,5]

[1]Graduate School of Engineering, Osaka University, Osaka, 565-0871, Japan, shiratsuchi@mat.eng.osaka-u.ac.jp
[2]Graduate School of Biomedical and Health Science, Hiroshima University, Hiroshima, 754-8553, Japan
[3]Research Center for Ultra-High Voltage Electron Microscopy, Osaka University, Osaka, 567-0047, Japan
[4]Institute for Open and Transdisciplinary Research Initiatives, Osaka University, Osaka, 565-0871, Japan
[5]Center for Spintronics Research Network, Osaka University, Osaka, 560-8531, Japan
[6]Institute for Protein Research, Osaka University, Osaka 565-0871, Japan

We synthesized Co-Pt nanoparticles in a crystal composed of proteins with a cage structure (i.e., *Pyrococcus furiosus* virus-like particle (PfV)) and investigated their magnetic interactions. When the soaking concentrations of metal, Co, and Pt ions in the PfV crystal were below 5.5 mM, isolated Co-Pt nanoparticles were formed. The size of the primary particles was 2-3 nm, which was smaller than the inner core size of the cage structure. When the soaking concentrations increased above 11 mM, the Co-Pt nanoparticles formed aggregates exceeding 30 nm in size. The synthesized nanoparticles showed superparamagnetic behavior at 300 K, independent of the soaking concentration. The temperature dependence of the AC magnetic susceptibility and remanent magnetization curve verified the occurrence of magnetic interactions between the Co-Pt nanoparticles. These measurements revealed that the dipolar-dipolar interaction was significant in the closely packed isolated nanoparticles, whereas it was weaker in the aggregated Co-Pt nanoparticles, probably due to the increased distance between the particles.

***Index Terms*—magnetic nanoparticle, superparamagnetism, protein crystal, dipolar interaction**

I. Introduction

Superparamagnetic nanoparticles combined with biomolecules (e.g., proteins) are promising for biological and medical applications, such as hyperthermia, drug delivery systems (DDS), magnetic particle imaging (MPI), and magnetic sensing [1-3]. To date, ferucarbotran, that is, Fe_3O_4/γ-Fe_2O_3 nanoparticles coated with carboxymethyl dextran, have been widely investigated, probably because it is one of few authorized magnetic nanoparticles for biomedical applications. The main target of ferucarbotran is cancer cells, the size of which is typically in the micrometer regime [1,3,4-7]. It is known that the ferucarbotran easily aggregates and forms the so-called multicore particles [5-9]; however, the increased core size is not necessarily problematic for cell detection, because the aggregate size is still sufficiently smaller than that of the target cell. On the other hand, there is also a demand for the highly sensitive detection of viruses, whose size is typically several 10 to 100 nm, much smaller than that of cells. Although virus detection using magnetic nanoparticles has been attempted using ferucarbotran [10,11], it would be suitable to tune the particle size to be comparable to that of the target virus, such as when we utilize Brownian motion as the detection principle. Magnetic nanoparticles encapsulated in virus-like particles (VLP) are important candidates for such applications. The size of VLPs is typically several tens of nanometers, which is comparable to that of viruses. VLPs are composed of proteins that directly capture foreign molecules and have a cage structure into which magnetic nanoparticles can be incorporated [12-14]. The *Pyrococcus furiosus* virus-like particle (PfV) [15,16], recently described as *Pyrococcus furiosus* encapsulin [14], is a promising candidate for this application [17,18] because of various advantages such as high thermal stability derived from the hyperthermophilic archaea [12,13,19]. The PfV particles are composed of 180 protein subunits and have an icosahedral symmetry. In the PfV structure, the initial residues (1-109 residues) do not have a specific ordered structure, thus yielding high flexibility to alter the amino acid and allowing the easy incorporation of the metal [18], e.g., recombinant PfV (hereafter referred to as rPfV).

Research on ferucarbotran suggests that multicore particles formed by the aggregation of several nanoparticles exhibit magnetic properties suitable for bioengineering applications [6-9]. The formation of multicore particles is strongly associated with the magnetic interactions between nanoparticles, i.e., exchange interactions or dipolar interactions. Magnetic interactions between nanoparticles have been widely explored, and various methods tackling this issue has been established [20-27]. In this study, we apply some of these techniques, such as AC magnetic susceptibility measurements and remanent magnetization measurements, to experimentally explore the magnetic interactions of Co-Pt nanoparticles synthesized in a PfV crystal.

II. Experimental

In this study, we used conventional magnetization measurement techniques for solids on an rPfV crystal. The rPfV crystal was expressed and purified using a previously reported method [17,18]. The crystallization of the rPfV crystal was performed using the hanging-drop vapor diffusion method at 20 °C. The crystals were grown in 2-3 μl drops containing a 1:1 (v/v) mixture of 20-30 mg/ml rPfV in 50 mM Tris-HCl (pH 7.5) and 150 mM NaCl and 29-30% 2-methyl-2,4-pentanodiol (MPD) in 100 mM Tris-HCl (pH 9.0). The metal ions were

soaked in the rPfV crystal; Co^{2+} from $Co(NH_4)_2(SO_4)_2 \cdot 6H_2O$ and $PtCl_4^{2-}$ from K_2PtCl_4 were used to synthesize the Co-Pt nanoparticles. The Co/Pt ratio was maintained at 1/3. To synthesize the nanoparticles, the soaked rPfV crystal was washed with a buffer solution to remove redundant ions, i.e., ions that were not captured by the rPfV crystal. $NaBH_4$ was applied to the washed rPfV crystals to reduce the metal ions. The total ion molar concentrations of $Co(NH_4)_2(SO_4)_2 \cdot 6H_2O$ and K_2PtCl_4 varied between 1.1 and 33 mM (millimol $\cdot L^{-1}$).

The structure of the rPfV crystal and synthesized Co-Pt nanoparticles was characterized using optical microscopy (OM) and transmission electron microscopy (TEM). TEM observations were performed to evaluate the structure of the Co-Pt nanoparticles using the unstained protein. The crystals were then crushed to allow electron transmission. The acceleration voltage was set to 200 kV.

The magnetic properties were characterized using DC and AC magnetization measurements. DC magnetization was measured using a superconducting quantum interference device (SQUID) magnetometer to obtain the magnetization curves. AC magnetization was measured using a physical property measurement system (Quantum Design. Inc). The AC magnetization was measured as a function of the temperature. The amplitude of the applied AC field was fixed at 10 Oe and the frequency was varied from 500 Hz to 10 kHz. The isothermal remanent magnetization (IRM) and DC demagnetization remanent magnetization (DCD) curves were measured at 10 K using the SQUID magnetometer to characterize the interparticle interaction. For the IRM measurements, the sample was cooled in a zero magnetic field from 300 to 10 K. At 10 K, a magnetic field was temporarily applied. The magnetic field was then removed, and the magnetization was measured. The temporarily applied magnetic field strength was varied from 0 to 20 kOe. The DCD curve was measured in a similar manner except for the cooling process. For the DCD measurements, the sample was cooled in a strong negative magnetic field of −50 kOe.

III. Results & Discussion

A. Nanoparticle formation in rPfV crystal

Figure 1 shows the OM images of the rPfV crystal at each treatment step. A hexagonal crystal with a long axis greater than 1 mm was obtained. A simple polyhedral shape without grain boundaries indicates the formation of a single crystal. In a previous study, the space group of the rPfV crystal had been determined as *I*23 based on synchrotron X-ray measurements [18]. Upon soaking and reduction, the outer shape of the rPfV crystal was maintained. In agreement with [18], the color of the crystal changed from transparent to brown upon ion soaking (Fig. 1(b)), and finally to black upon reduction (Fig. 1(c)).

Figure 1 Optical microscopy images of rPfV crystal at each step: (a) as made, (b) after soaking, and (c) after reduction.

Figures 2(a)-2(e) show TEM images of the Co-Pt nanoparticles synthesized in the rPfV crystal; rPfVs were not visualized because of the low atomic weight of the constituent elements in the protein. When the soaking concentration was below 5.5 mM (Figs. 2(a)-2(c)), isolated nanoparticles with approximate diameters of 2-3 nm were observed, independent of the soaking concentration. Fig. 2(f) shows a cross-sectional view of the PfV particle. In the icosahedral symmetry (point group 532), and the inner diameter along each symmetry axis is also shown in Fig. 2(f). Compared to the PfV size, the formed nanoparticles were sufficiently small to be incorporated inside the cage structure. As the soaking concentration increased but remained below 5.5 mM, the number and density of nanoparticles increased. At a concentration of 5.5 mM, the formed nanoparticles were closely packed, and the inter-particle distance was approximately 3.5 nm. At a soaking concentration of 11 mM (Figs. 1(d), (e)), the primary nanoparticles aggregated.

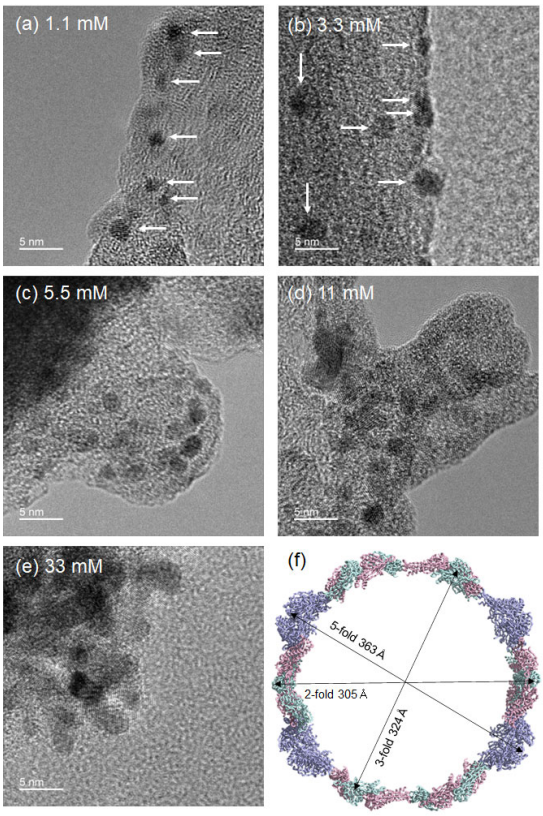

Figure 2 TEM images of Co-Pt nanoparticles synthesized in the rPfV crystal. The soaking concentration was (a) 1.1 mM, (b) 3.3 mM, (c) 5.5 mM, (d) 11 mM, and (e) 33 mM. (f) shows the schematic drawing of the cross-sectional view of the PfV particle [18] (Protein data bank 2E0Z). The relative size of the PfV crystal shown in (f) is matched with the scale bar in (a)-(e). Nanoparticles are indicated by white arrows in (a) and (b).

The sizes of the aggregated nanoparticles increased along with the soaking concentrations. Aggregated particles larger than 30 nm were formed at 33 mM. the sizes of which surpassed the inner core size of the rPfV. These particles were formed outside the individual rPfV, inducing the collapse of the crystal structure, as confirmed by synchrotron X-ray diffraction analysis (not shown).

Regarding the exact Co-Pt composition of the formed nanoparticles, in principle, this can be estimated from, e.g., the lattice spacing. However, this topic remains to be investigated.

B. Superparamagnetism behavior and magnetic interaction between nanoparticles

Figure 3(a) shows the magnetization curve measured at 300 K under a soaking concentration of 33 mM. When the soaking concentration was below 3.3 mM, the magnetization could not be detected because of the small amount of magnetic entities. The magnetic response at 300 K was nonlinear, indicating the presence of a noticeable magnetic moment in the rPfV crystal. The remanent magnetization and coercivity were both zero (see inset of Fig. 3(a)), and the magnetization approached saturation above 50 kOe. In conjunction with the nanoparticle formation shown in Fig. 2, the *M-H* curve signified superparamagnetic behavior.

Figure 3(b) shows the temperature dependence of the real part of the AC susceptibility. The AC susceptibility increased along with the temperature, reached a peak, and then decreased again. The peak temperature, T_{peak}, is generally defined as the blocking temperature below which the magnetization direction is blocked within the measurement timescale. As shown in the inset of Fig. 3(a), the coercivity (~0.5 kOe) and remanence observed at 10 K supported the occurrence of superparamagnetism at 300 K and the blocking of magnetization below T_{peak}. Notably, the magnetization significantly increased at 10 K because the nonlinear magnetic response from the unreduced Co^{2+} was superimposed [18]. The magnetization relaxation time τ (= $1/f$) is expressed as follows:

$$\tau = 1/f = \tau_0 \exp\left(-\frac{\Delta E}{k_B T}\right) \quad (1)$$

where τ_0 is a prefactor (typically 10^{-9}-10^{-12} s), ΔE is the energy barrier for the magnetization reversal, k_B is the Boltzmann factor, and T is the absolute temperature. As expected from eq. (1), T_{peak} shifted toward higher values at higher AC field frequencies, as shown in Fig. 3(b). Based on the hypothesis that ΔE is constant, the frequency dependence of T_{peak} yields ΔE; however, ΔE for the interacting nanoparticles can be complicated, and its precise expression is nontrivial. Moreover, ΔE depends on the assumed value of τ_0. As originally discussed by Néel and derived in [28], τ_0 depends on various parameters, such as the magnetic anisotropy energy density, anisotropy field, and temperature. A precise τ_0 value requires careful treatment and is a long-standing issue. However, the monotonic increase of T_{peak} with f (inset of Fig. 3(b)) suggests that the temperature dependence of τ_0 is not very large, at least near the peak temperature. Here, we evaluated the magnetic interaction between the magnetic nanoparticles using the Mydosh parameter, which is defined as follows [29]:

$$\xi = \frac{\Delta T_{peak}}{T_{peak} \Delta \log_{10} f} \quad (2)$$

The Mydosh parameter is dimensionless and is less affected by the τ_0 value. As seen in the inset of Fig. 3(b), T_{peak} shows a linear increase as a function of $\log_{10} f$. Using the f range from 630 Hz to 10 kHz, the ξ value was deduced as 0.06 ± 0.01. For noninteracting isolated nanoparticles, the ξ value is above 0.1 [20], and for a system with an interparticle interaction or a spin-glass-like nature, the ξ value is below 0.1 [24,30]. In particular, the spin-glass-like behavior in strongly interacting systems shows a small ξ in the order of 10^{-2} to 10^{-3}. The intermediate ξ value in the middle of 10^{-2} suggests the presence of interparticle interactions, while the increase in ξ is related to the decrease in interparticle interaction.

We reinforce the presence of interparticle interactions based on IRM and DCD measurements and examined the effect of Co-Pt concentration on the strength of the interparticle interactions. When isolated nanoparticles show a coherent rotation of magnetization reversal, the IRM and DCD measurements are related by the Wohlfarth relationship [31]:

$$m_D(H) - [1 - 2m_R(H)] = 0 \quad (3)$$

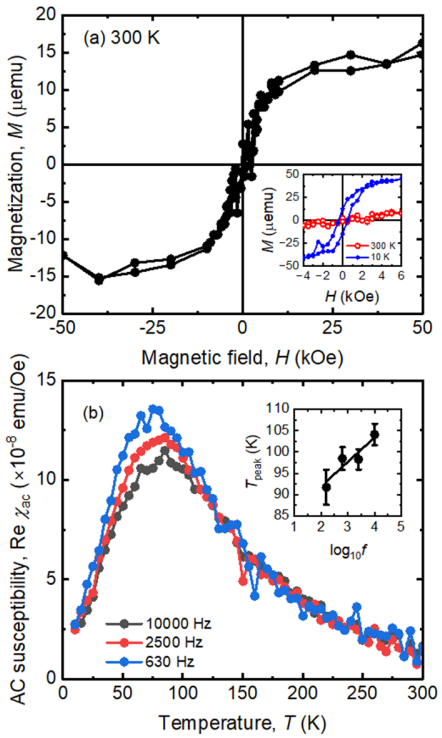

Figure 3 (a) Magnetization curve measured at 300 K. Inset shows the enlarged *M-H* curve; the curve measured at 10 K is also shown. (b) Temperature dependence curve of real part of AC susceptibility. The frequency of the AC magnetic field was 630 Hz (blue), 2500 Hz (red), and 10000 Hz (black). The inset of (b) shows the $\log_{10} f$ dependence of T_{peak}. The applicable soaking concentration in this figure is 33 mM.

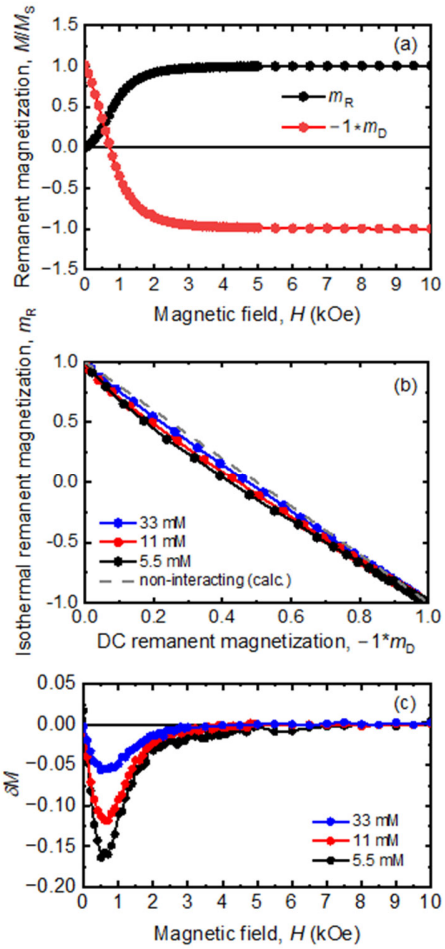

Figure 4 (a) Remanent magnetization curve measured at 10 K for the sample synthesized under a 5.5 mM soaking concentration. (b) Henkel plots and (c) δM plots for the samples synthesized under soaking concentrations of 33 mM (blue), 11 mM (red), and 5.5 mM (black). Gray broken line in (b) represents the Wohlfarth relationship for the non-interacting particles represented by Eq. (3).

where $m_D(H)$ and $m_R(H)$ are DCD and IRM normalized by their saturation values, respectively. The direct relationship between $m_D(H)$ and $m_R(H)$ is referred to as the Henkel plot [22,25]. For interacting particles, the Wohlfarth relation is not preserved, and the Henkel plot deviates from a straight line. The upward (downward) deviation from the straight line indicates interactions favoring the magnetizing (demagnetizing) state associated with the predominant exchange interaction (dipolar interaction). The relationship between $m_D(H)$ and $m_R(H)$ can be observed more clearly by plotting δM defined as the left side of eq. (3) as a function of the magnetic field, that is, the δM plot [21]. In the δM plot, the exchange and dipolar interactions manifest as positive and negative deviations from zero, respectively.

Figure 4(a) shows typical examples of IRM and DCD curves collected for Co-Pt nanoparticles with a soaking concentration of 5.5 mM. Based on the above measurement process, $-1*m_D(H)$ is plotted in Fig. 4. The IRM curve started from zero and gradually approached positive saturation with an increasing magnetic field. The DCD curve started from almost 1, monotonically decreased, and approached negative saturation with the increasing magnetic field. These magnetic responses of remanent magnetization have been widely observed in magnetic nanoparticles [24]. Figures 4(b) and 4(c) show the Henkel and δM plots for the three samples. For all the samples, the Henkel plots showed a downward deviation from the straight line, and δM was negative, indicating a behavior favoring demagnetization associated with a dominant contribution of dipolar interactions. However, there is a report that the δM plot possibly show a dip even for isolated particles [32]. This type of dip has been reported for magnetite nanoparticles and is attributed to the exchange coupling of disordered surface spins with a uniform ferrimagnetic core. Disordered surface spins sometimes exist in oxide nanoparticles [32,33], whereas they are unlikely to exist in metallic nanoparticles. This is probably because an inhomogeneity of the surface spin configuration can occur in the oxide, where the exchange interaction is sensitive to structural disordering owing to the predominance of super-exchange interactions via O^{2-}. In contrast, exchange coupling in metallic nanoparticles is mainly caused by direct exchange coupling, in which the exchange length is shorter than that in oxides. In metallic nanoparticles, the inhomogeneous spin configuration incurs high energy costs owing to exchange coupling. Therefore, in our case, the dip in δM due to the surface spin disordering should be a minor effect, even if that was the case.

The dip in the δM plot deepened with the decreasing soaking concentration, indicating a stronger dipolar interaction for lower soaking concentrations. Finally, we qualitatively discuss the changes in the dipolar interaction in conjunction with the structural changes. The dipolar interaction energy E_{dip} between magnetic moments $\boldsymbol{m}_1$ and $\boldsymbol{m}_2$ separated by vector $\boldsymbol{r}$ is expressed as follows:

$$E_{dip} = \frac{1}{4\pi\mu_0 r^3}\left[\boldsymbol{m}_1 \cdot \boldsymbol{m}_2 - \frac{3(\boldsymbol{m}_1 \cdot \boldsymbol{r})(\boldsymbol{m}_2 \cdot \boldsymbol{r})}{r^2}\right] \quad (4)$$

where μ_0 is the magnetic permeability of vacuum. On the rough hypothesis of $|\boldsymbol{m}_1| = |\boldsymbol{m}_2| = m$ and $\boldsymbol{m}_1 // \boldsymbol{m}_2$, the dipolar interaction is proportional to m^2 and r^{-3}. Therefore, E_{dip} was more sensitive to r than m. According to the structural analysis shown in Fig. 2, a low soaking concentration, e.g., 5.5 mM, gives rise to isolated nanoparticles, inducing a high nanoparticle packing density. A small distance between individual nanoparticles results in strong dipolar interactions. In contrast, when the nanoparticles aggregated under a high soaking concentration (e.g., 33 mM), the aggregated particles behaved as single magnetic particles. The reduction in the dipolar interaction suggests that the magnetic behavior of a large single particle is prominent, and the dipolar interaction is weak because of the large distance between particles. We cannot rule out the presence of exchange interactions within the aggregated particles due to the physical contact between nanoparticles. A more quantitative analysis associated with structural analysis will be helpful for a deeper understanding of the magnetic interaction in future studies.

IV. Summary

We investigated the structural and magnetic properties of Co-Pt nanoparticles synthesized within a cage-structured protein. The primary nanoparticles were typically a few nanometers in diameter, which seemed to be independent of the metal ions concentration. The nanoparticles remained isolated at soaking concentrations below 5.5 mM, whereas above 11 mM they started to aggregate. All studied samples exhibited superparamagnetic properties at 300 K. The presence of interparticle interactions was inferred from the Mydosh parameter deduced from the AC susceptibility measurements, Henkel plot, and δM-plot. The Mydosh parameter for the aggregated particles synthesized with 33 mM Co-Pt was approximately 0.06, which is an intermediate value between the strong interaction, $<10^{-2}$, and the non-interacting nanoparticles (>0.1). The Henkel plot and δM-plot indicated that the dipolar interaction was predominant, and the strength increased as the soaking concentration decreased. A more qualitative analysis associated with the structural analysis, that will be conducted in the future, will provide deeper insights.

Acknowledgments

This study was partially supported by JSPS KAKENHI (Grant No. 22K18903). This study was supported in part by the Collaborative Research Program of Institute for Protein Research, Osaka University, CR-16-05, CR-18-05, CR-19-05, CR-20-05, CR-21-05, and CR-22-05.

References

[1] Q. A. Pankhurst, J. Connolly, S. K. Jones, and J. Dobson, "Application of magnetic nanoparticles in biomedicine" *J. Phys. D: Appl. Phys.* Vol. 36, pp. R167-R181 (2003).

[2] A. K. Gupta and M. Gupta, "Synthesis and surface engineering of iron oxide nanoparticle for biomedical applications." *Biomaterials* Vol. 26, pp. 3995 – 4021 (2005).

[3] S. Laurent, D. Forge, M. Port, A. ROch, C. Robic, L. V. Elst, and R. N. Muller, "Magnetic iron oxide: synthesis, stabilization, vectorization, physicochemical characterization, and biological applications." Chem. Rev. Vol. 108, pp. 2064 – 2110 (2008).

[4] S. Moret, S. Vasseur, F. Grasset, and E. Doguet, "Magnetic nanoparticle design for medical diagnosis and therapy." *J. Mater. Phys. Chem.* Vol. 14, pp. 2161-2175 (2004).

[5] S. Ota, S. B. Trisnanto, S. Takeuchi, J. Wu, Y. Cheng and Y. Takemura, "Quantitation method of loss powers using commercial magnetic nanoparticles based on superparamagnetic behavior influenced by anisotropy for hyperthermia." J. Magn. Magn. Mater. Vol. 538, pp. 168313 (2021).

[6] C. Lu, X. Xu, T. Zhang, Z. Wang, and Y. Chai, "Biocompatible and superparamagnetic Manganese doped iron oxide nanoclusters for diagnostic applications." ACS Appl. Nano Mater. Vol. 5, pp. 2541-2549 (2022).

[7] H. Kartz, M. Taupitz, A. Ariza de Schellenberger, D. Eberbeck, S. Wagner, L. Trahms, B. Hamm, and J. Shonorr, "Novel magnetic multicore nanoparticles designed for MPI and other biomedical applications: From synthesis to first in vivo studies" PLOS ONE Vol. 13, pp. e190214 (2018).

[8] D. Eberbeck, C. L. Dennis, N. F. Huls, K. L. Kryn L. Krycka, C. Grüttner, and F. Westphal, "Multicore magnetic nanoparticles for magnetic particle imaging." IEEE Trans. Magn. Vol. 49, pp. 269-274 (2013).

[9] S. Dutz, J. H. Clement, D. Eberbeck, T. Gelbrich, R. Hergt, R. Müller, J. Wostchadlo, and M. Zeisberger, "Ferrofluids of magnetic multicore nanoparticles for biomedical applications" J. Magn. Magn. Mater. Vol. 321, pp. 1501-1504 (2009).

[10] S. H. Chung, A. Hoffmann, S. D. Bader, S. Liu, B. Kay, L. Makowski, and C. Chen, "Biological sensors based on Brownian relaxation of magnetic nanoparticles." Appl. Phys. Lett. Vol. 85, pp. 2971-2973 (2004).

[11] R. Hirota, T. Maruyama, R. Katsumi, T. Kawawaki, S. Yabukami, R. Igarashi, Y. Negishi, M. Kusakabe, M. Sekino, T. Yatsui, and A. Kuwahata, "Rapid virus detection using magnetic second harmonics of superparamagnetic iron oxide nanoparticles." *AIP Advances* Vol. 13, pp. 025144 (2023).

[12] F. C. Meldrum, V. J. Wade, D. L. Nimmno, B. R. Heywood, and S, Mann, "Synthesis of inorganic nanophase materials in supermolecular protein cases." *Nature* Vol. 349, pp. 684-687 (1991).

[13] F. C. Meldrum, B. R. Heywood, and S. Mann, "Magnetoferritin: In vitro synthesis of a novel magnetic protein." *Science* Vol. 257, pp. 522-523 (1992).

[14] A. V. Almeida, A. J. Carvalho, and A. S. Pereira, "Encapsulin nanocages: Protein encapsulation and iron sequestration." *Coordination Chemistry Reviews* Vol. 448, pp. 214188 (2021).

[15] K. Namba, K. Hagiwara, H. Tanaka, Y. Nakanishi, K. T. Chong, E. Yamashita, G. E. Armah, Y. Ono, Y. Ishino, T. Omura, T. Tsukihara, and A. Nakagawa, J. Biochem. 138, 193 (2005).

[16] F. Akita, K. T. Chong, H. Tanaka, E. Yamashita, N. Miyazaki, Y. Nakanishi, M. Suzuki, K. Namba, Y. Ono, T. Tsukihara and A. Nakagawa, J. Mol. Biol. 368, 1469. (2007).

[17] Y. Shiratsuchi, F. Nishiura, K. Tachibori, A. Higashiura, A. Nakagawa, R, Nakatani, T. Tsukihara, and M. Yamamoto, J. Mag. Soc. Jpn. 33, 473 (2009).

[18] M. Taniguchi, A. Higashiura, N. Kobayashi, D. Kanda, K. Tagata, R. Fukunishi, Y. Yoshikawa, E. Kuromatsu, N. Koshida, Y. Kotani, K. TOyoki, T. Nakamura, R. Nakatani, A. Nakagawa, and Y. Shiratsuchi, "Synthesis of superparamagnetic Co-Pt nanoparticle in *Pyrococcus furiosus* virus-like particle crystal." *J. Phys. Chem. Solids* Vol. 169, pp. 110840 (2022).

[19] A. Higashiura *et al*., to be submitted.

[20] J. L. Dormann, L. Bassais, and D. Fiorani, "A dynamic study of small interacting particles: superparamagnetic model and spin-glass laws" *J. Phys. C: Solid State Phys.* Vol. 21, pp. 2015-2034 (1988).

[21] P. E. Kelly, K. O'Grady, P. I. Mayo, and R. W. Chantrell, "Switching mechanisms in cobalt-phosphorus thin films." IEEE Trans. Magn. Vol. 25, pp. 3881-3883 (1989).

[22] I. Klik, Y. D. Yao and C. R. Chang, "Henkel plots for thermally relaxing systems." J. Appl. Phys. Vol. 81, pp. 5230-5232 (1997).

[23] Y. Shiratsuchi and M. Yamamoto, "Dominant factor of zero-field-cooled magnetization in discontinuous Fe films" Phys. Rev. B Vol. 76, pp. 144432 (2007).

[24] C. A. Vieira, R. Cabreira Gomes, F. G. Silva, A. L. Dias, R. Aquino, A. F. C. Campos, and J. Depeyrot, "Blocking and remanence properties of weakly and highly interactive cobalt ferrite based nanoparticles." *J. Phys. Condens. Matter* Vol. 31, pp. 175801 (2019).

[25] J. García-Otero, M. Porto, and J. Rivas, " Henkel plots of single-domain ferromagnetic particles." J. Appl. Phys. Vool. 87, pp. 7376-7381 (2000).

[26] D. Slay, D. Cao, E. C. Ferré, "Ferromagnetic resonance of superparamagnetic nanoparticles: Th effect of dipole-dipole interactions." *J. Appl. Phys.* Vol. 130, pp. 113902 (2021).

[27] S. B. Trisnanto and Y. Takemura, "Effective Néel relaxation time constant and intrinsic dipolar magnetism in a multicore nanoparticle system." *J. Appl. Phys.* Vol. 130, pp. 063302 (2021).

[28] M. El-Hilo, K. O'Grady, and R. W. Chantrell, "Susceptibility phenomena in a fine particles system: II. Field dependence of the peak" *J. Magn. Magn, Mater.* 114, 307 (1992).

[29] J. A. Mydosh, "Spin glasses: redux: an updated experimental/materials survey." *Res. Prog. Phys.* Vol. 78, pp. 052501 (2015).

[30] K. Konwar, S. D. Kaushik, D. Sen, and D. Deb, "Dynamic spin freezing and magnetic memory effect in ensembles interacting anisotropic magnetic nanoparticles." *Phys. Rev. B* Vol. 102, pp. 174449 (2020).

[31] E. P. Wohlfarth, "Relations between different modes of acquisition of the remanent magnetization of ferromagnetic particles." J. Appl. Phys. Vol. 29, pp. 595-596 (1958).

[32] J. A. De Toro, M. Vasikakaki, S. Seong Lee, M. S. Andersson, P. S. Normile, N. Yaacoub, P. Murray, E. H. Sánchez, P. Muñiz, D. Peddis, R. Mathieu, K. Liu, J. Gashev, K. N. Trohidou, and J. Nogués, "Remanence plots as a probe of spin disorder in magnetic nanoparticles." Chem. Mater. Vol. 29, pp. 8258-8268 (2017).

[33] R. H. Kodama, "Magnetic nanoparticles." J. Magn. Magn. Mater. Vol. 200, pp. 259-372 (1999).